Infrared mapping of ultrasound fields generated by medical transducers: Feasibility of determining absolute intensity levels

Vera A. Khokhlova[a)]
University of Washington, Center for Industrial and Medical Ultrasound, Seattle, Washington 98105

Svetlana M. Shmeleva[b)]
Department of Medical Physics, Moscow State University, Physics Faculty, Moscow 119991, Russia

Leonid R. Gavrilov
N. N. Andreyev Acoustics Institute, Moscow 117036, Russia

Eleanor Martin, Neelaksh Sadhoo, and Adam Shaw
National Physical Laboratory, Acoustics and Ionizing Radiation Division, Teddington TW11 0LW, United Kingdom

(Received 12 October 2012; revised 6 March 2013; accepted 15 March 2013)

Considerable progress has been achieved in the use of infrared (IR) techniques for qualitative mapping of acoustic fields of high intensity focused ultrasound (HIFU) transducers. The authors have previously developed and demonstrated a method based on IR camera measurement of the temperature rise induced in an absorber less than 2 mm thick by ultrasonic bursts of less than 1 s duration. The goal of this paper was to make the method more quantitative and estimate the absolute intensity distributions by determining an overall calibration factor for the absorber and camera system. The implemented approach involved correlating the temperature rise measured in an absorber using an IR camera with the pressure distribution measured in water using a hydrophone. The measurements were conducted for two HIFU transducers and a flat physiotherapy transducer of 1 MHz frequency. Corresponding correction factors between the free field intensity and temperature were obtained and allowed the conversion of temperature images to intensity distributions. The system described here was able to map in good detail focused and unfocused ultrasound fields with sub-millimeter structure and with local time average intensity from below 0.1 W/cm^2 to at least 50 W/cm^2. Significantly higher intensities could be measured simply by reducing the duty cycle. © *2013 Acoustical Society of America*.
[http://dx.doi.org/10.1121/1.4812878]

PACS number(s): 43.80.Vj, 43.35.Yb, 43.58.Fm, 43.58.Vb [CCC] Pages: 1586–1597

I. INTRODUCTION

Recently, high intensity focused ultrasound (HIFU) has been investigated extensively as a medical technology for noninvasive ablation of deeply located tumors. HIFU systems based on the use of a single focused transducer and multiple element phased arrays have been proposed to scan a single focus or to generate several foci simultaneously in clinically relevant volumes of tissue. So, measurement of acoustical fields of HIFU transducers is a problem of high importance.[1,2] Various methods can be employed, such as hydrophones, thermocouples, magnetic resonance imaging (MRI), and ultrasound thermometry, to measure the spatial distributions of pressure or intensity in water. There has been considerable interest in using the infrared (IR) technique to investigate the acoustical fields of HIFU transducers[3–5] which seems to have increased in recent years.[6–12] The IR method has specific advantages in comparison with these other methods. Hydrophone field mapping in three dimensions is very slow, with even a single planar raster scan taking typically several hours. In addition, hydrophones and thermocouples are local sensors which must be placed at each point of interest in the ultrasound field; MRI is expensive, and both MRI and ultrasound thermometry have poor accuracy and spatial resolution compared to thermocouples. Experiments with two-dimensional (2D) phased arrays that offer electronic steering of a single focus and formation of patterns of multiple foci imply the need to measure a large number of intensity distributions. Using a scanned hydrophone in this particular situation would be prohibitively slow taking into account the potentially large number of focusing conditions. Moreover, hydrophones that are used for field mapping can be damaged in some HIFU fields.

A common feature of previous studies on the application of IR-scanners for visualization of temperature rise caused by absorption of ultrasound was to use two blocks of

[a)]Also at: Moscow State University, Physics Faculty, Department of Acoustics, Moscow 119991, Russia.
[b)]Author to whom correspondence should be addressed. Electronic mail: sveta@acs366.phys.msu.ru

tissue-mimicking phantom or tissue which were stacked and their interface was placed along or across the axis of an ultrasound beam.[3–5] After exposure to ultrasound, the upper piece was immediately removed and the temperature on the surface of the phantom or tissue was IR imaged. Theoretical predictions of temperature distributions agreed qualitatively with those obtained with the IR camera.

Based on the principle that temperature in a medium increases most quickly where the intensity is the highest, a technique for rapid qualitative assessment of intensity distributions in water was developed by Shaw and Nunn which enables mapping of the ultrasound field in a time on the order of seconds or even tenths of a second.[7] The principle has been applied to measure the relative intensity distribution of a multiple element random phased array by measuring the distribution of the initial rate of temperature increase at the start of insonation.[6,11,12] The temperature rise was measured in a thin (<2 mm thick), highly absorbing (30 dB cm^{-1} MHz^{-1}) polyurethane layer with an IR camera. In this study, the assumption was that the measured temperature rise at the surface of the absorber is proportional to the free field intensity. Other studies have extended the method to account for the effect of heat diffusion by introducing correction factors in the conversion of temperature images to intensity,[8,9,11,12] and measuring the temperature distribution on the surface of a thick (40 mm) less absorbing tissue mimicking gel (0.6 dB cm^{-1} MHz^{-1}).[10] Good correlation between the IR measurements and modeled results in both spatial distributions and the absolute values of intensity was claimed in these previous studies.

The present paper is the continuation of work, initiated in the papers Bobkova *et al.* and Shaw *et al.*, where the method to estimate the absolute values of intensity from the IR temperature measurements was proposed.[8,12] The temperature rise measured in an absorber with the use of an IR camera was correlated with the pressure distribution measured in water using a calibrated hydrophone. The measurements were performed for a flat physiotherapy transducer and two focused HIFU transducers. Calibration factors between the free field intensity in water and temperature measured at the absorber/air interface were obtained and allowed the conversion of temperature images to intensity distributions. A number of practical measurement considerations were addressed relating to interference caused by the presence of a reflecting absorber and air interface.

II. METHODS

Three radiators with frequencies close to 1 MHz were studied as this frequency is commonly used in ultrasound therapy. Intensity distributions reconstructed from IR images were compared with direct hydrophone measurements to validate the accuracy of the method as a means of determining the absolute value of temporal-average intensity.

A. IR system for visualization of ultrasound fields

IR measurements were carried out using a modified ThermoScope® pulsed thermography system (Thermal Wave Imaging Inc., Ferndale, MI) that included a Phoenix MWIR 9705 IR camera (FLIR Systems, Boston, MA), and a PC running EchoTherm® v6.4 software following the procedure described by Hand *et al.*:[6] A diagram of the experimental arrangement is shown in Fig. 1. The ultrasound beam was directed vertically upwards through water onto a layer of ultrasonic absorber (Aptflex F28, Precision Acoustics, Dorchester, UK) of 2 mm thickness with a single-pass attenuation coefficient of 6 dB at 1 MHz ultrasound frequency.[8] The reflection of ultrasound at the water/absorber interface was −25 dB.[8] The other side of the absorber was air-backed (fully reflective to ultrasound) and viewed from above by the IR camera. The thermal resolution of the IR image was 5.6 mK and the pixel size was 0.25 mm. The measured raw IR signal expressed in binary levels was approximately 180 levels per degree Celsius and the thermal noise level (expressed as a standard deviation at an individual image pixel) was typically three levels. The typical peak value of the IR signal change was between 500 and 1000 levels over 0.2 s, so the signal-to-noise ratio was typically more than 100 around the peaks in the distribution. The position of the transducer relative to the absorber along the beam axis was adjusted using a micrometer positioning stage with a 50 mm range of displacement. In this setup, unlike for the hydrophone measurements, there is no absolute measure of the distance from the radiating surface to the top of the absorber. The absolute position was estimated by touching the underside of the absorber with the rim of the transducer housing so there is a positioning uncertainty of approximately ±1 mm.

The generation of signals applied to the transducer was provided by a function generator (Agilent 33250A, Agilent Technologies, Palo Alto, CA) and an amplifier (A300, Electronics and Innovation, Rochester, NY). To avoid interference from reflected acoustic waves between the absorber/air interface and the transducer, which can happen when the transducer is driven in continuous mode of excitation, insonation was performed using a tone burst mode. The duration and repetition period of the tone bursts were chosen depending on the distance between the absorber and transducer. For

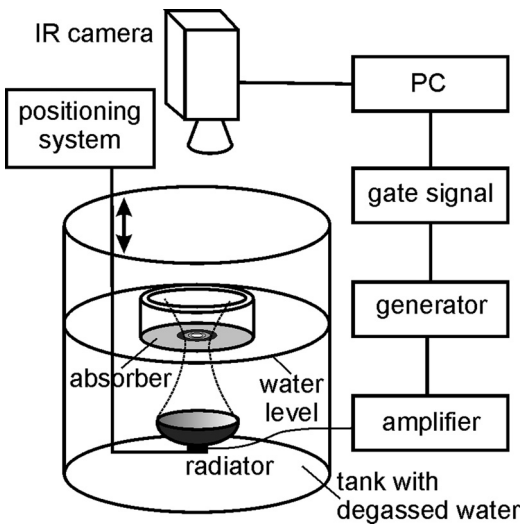

FIG. 1. IR system for visualization of ultrasound fields.

the distance z between the reflecting interface and the transducer, the burst repetition period was chosen as $6z/c$, and the burst duration was $2.4 \cdot z/c$ (0.4 duty factor). The burst duration varied from the minimum value of 16.2 μs ($z = 10$ mm) to the maximum value of 226 μs ($z = 140$ mm). Generation of the tone bursts was provided by a second function generator (HP8116A, Hewlett-Packard Corp., Palo Alto, CA).

The experimental system and software provided a method of acquiring, viewing, and saving IR images. The system was configured to capture a sequence of 60 frames at a rate of 50 fps, with the ultrasound exposure starting at the tenth frame of the IR measurement. The absorber was insonated over a period of 0.2 s. The sequence of frames was stored as a movie in the native Echotherm format to preserve the maximum dynamic range for later analysis. The distribution of temperature rise at the absorber/air interface was derived from the subtraction of the 11th from the 21st frame with the noise level in the subtracted image frame being typically 5 pixels, expressed as a standard deviation.

B. Experimental setup used for hydrophone measurements

The diagram of the experimental arrangement used for hydrophone measurements is shown in Fig. 2. The measurements were performed in a large acrylic water tank (approximately 100 cm × 50 cm × 40 cm) at room temperature (20 °C). The water was distilled and degassed under vacuum prior to measurements using a degassing system to limit cavitation during measurements. The transducer was driven with tone bursts using a generator (Agilent 33220A, Agilent Technologies, Palo Alto, CA) and an amplifier (A300, Electronics and Innovation, Rochester, NY). The drive voltage to the transducer was monitored during experiments with a high impedance probe. The pressure amplitude at the face of the transducer was proportional to the driving voltage, which was validated by radiation force balance measurements performed in previous studies. The pressure field was sampled by a capsule hydrophone (type HGL-0200, Onda Corporation, Sunnyvale, CA) with a 0.2-mm active element diameter. This type of hydrophone was preferred over a membrane type because a membrane presents a much larger reflecting area and the mounting ring could be a source of unwanted reflections when placed close to a transducer of similar diameter. The hydrophone was connected to an oscilloscope (DPO 7254, Tektronix Inc., Beaverton, OR) *via* a preamplifier (type AH-2020-DCBSW, Onda Corporation, Sunnyvale, CA): The overall sensitivity of the hydrophone measurement system at 1 MHz was 218 nV/Pa. Both the transducer and the hydrophone were attached to a positioning system that allowed alignment and movement within the tank with a precision of approximately 25 μm. The system was controlled by a computer using a LabView program (National Instruments, Austin, TX) written at NPL. The program recorded the hydrophone signal transferred from the oscilloscope and carried out a raster scan in a plane perpendicular to the beam axis with specified spatial resolution and window size. The window sizes used in the experiment were 40, 50, and 60 cm depending on the distance of the plane from the transducer, and the spatial increment was 0.2 or 0.4 mm. Axial scans were performed with 0.1 mm steps: The absolute distance from the radiating surface to the hydrophone was determined from the arrival time of the acoustic pulse at the hydrophone placed in the focus.

To avoid interference from acoustic reflections, a gated sine wave was used to drive the transducer. The trigger delay of the oscilloscope was adjusted so as to sample the signal after continuous wave (CW) behavior had been established, but before any reflections had returned from possible reflectors (hydrophone mount, back sides of the tank, etc.). The transducers were driven at a level which was low enough so that the magnitude of the nonlinear second harmonic in the focus was less than 5% of the fundamental one.

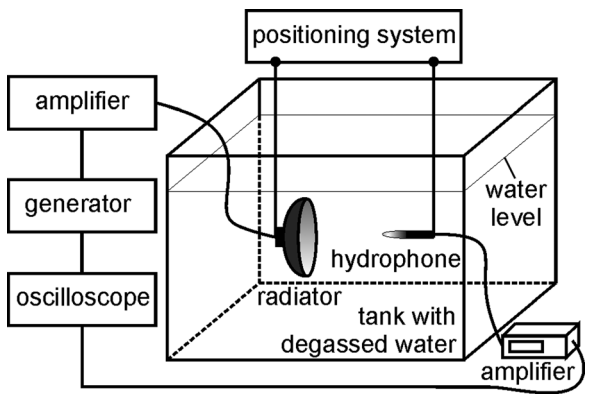

FIG. 2. A diagram of the experimental arrangement used for hydrophone measurements.

C. Ultrasound radiators used for calibration

Three radiators with close operational frequencies were used in the experiment: Photos of the radiators are shown in Figs. 3(a)–3(c). The first source [Fig. 3(a)] was a single element flat physiotherapy transducer (Enraf-Nonius B.V., Netherlands) with a resonant frequency of 1.022 MHz and a radiating surface of 5 cm^2. The second source [Fig. 3(b)] (on loan from the Institute for Cancer Research) was a homemade transducer with a spherically focused surface and a resonant frequency of 1.07 MHz, an aperture of 60 mm, and 120 mm radius of curvature. The third source [Fig. 3(c)] was a spherically focused piezoceramic HIFU transducer (type H101, Sonic Concepts, Bothell, WA) with a resonant frequency of 1.1 MHz. The transducer had a 64 mm aperture and 62.4 mm radius of curvature. The latter two are typical single element HIFU sources.

FIG. 3. (Color online) Ultrasound radiators used in experiments: (a) Flat physiotherapy transducer ENRAF, $f = 1.022$ MHz; (b) HIFU transducer ICR, $f = 1.07$ MHz; (c) HIFU transducer Sonic Concepts H101, $f = 1.1$ MHz.

D. Calculation of the calibration coefficient

The calibration coefficient can be determined by comparing the temperature calculated from hydrophone measurements of intensity with measurements of temperature made with the IR camera. First, it is necessary to establish the appropriate relationships and the assumptions underpinning them.

Following the results obtained in the previous publication,[8] it was known that at a short insonation time of $\Delta t = 0.2$ s, the effect of heat diffusion across the beam is negligible and the temperature rise ΔT at a location on the absorber surface is approximately proportional to the free field intensity in water at the same location in the same plane in the absence of the absorber:

$$\Delta T = kI_{ta}\Delta t = k\frac{p_{\text{hydr}}^2}{\rho\, c}\Delta t, \tag{1}$$

where k is the unknown coefficient, I_{ta} is the intensity distribution in the measurement plane, $\Delta t = 0.2$ s is the exposure time, p_{hydr} is the root-mean-square pressure measured with the hydrophone, $\rho = 1000\,\text{kg/m}^3$, and $c = 1484$ m/s are the density and sound velocity in water at room temperature. The unknown coefficient k is expected to depend on ultrasound frequency, the material properties, and thickness of the absorber but, for the purposes of the following derivation, it is assumed to be constant for a particular experimental configuration. This simplification is addressed in Sec. IV.

If diffusion effects across the measurement plane can be neglected and the camera optics and detector are assumed to be nearly ideal, then the temperature rise recorded by the IR camera in each pixel of the image is proportional to the change in the IR camera signal during exposure to ultrasound

$$\Delta T = h \cdot A_{\text{IR}}, \tag{2}$$

where A_{IR} is the IR camera signal (quantized in dimensionless *levels*) obtained by the subtraction of the 11th from the 21st frames, and h is an unknown coefficient that depends on camera settings as well as emissivity properties of the absorber but is expected to be constant for a particular configuration.

In practice, drive voltages to the transducer were different for the IR (V_{IR}) and for the hydrophone (V_{hydr}) measurements. The expected temperature rise in Eqs. (1) and (2), which is proportional to the intensity of the field, therefore should be normalized by the corresponding drive voltages squared. Accounting also for the duty factor of 0.4 in insonations of the absorber in IR measurements, the calibration factor k/h can now be determined from a set of measurable quantities

$$\frac{k}{h} = \frac{A_{\text{IR}}}{0.4 \cdot \Delta t} \cdot \frac{\rho\, c}{p_{\text{hydr}}^2} \cdot \left(\frac{V_{\text{hydr}}}{V_{\text{IR}}}\right)^2. \tag{3}$$

The sensitivity k/h is the rate of IR signal increase per unit intensity and has units of (levels/s)/(W/m^2).

E. Field model

For completeness, pressure distributions in the field of the transducers were also modeled assuming linear propagation of ultrasound and compared with low amplitude hydrophone measurements in water along the beam axis. The modeling was based on the well understood and commonly used piston source model of circular symmetry: The source amplitude distribution of the vibration velocity was considered to be uniform within a diameter equal to the effective diameter of the transducer element. The corresponding pressure distribution along the axis in water was calculated using the Rayleigh integral.[8] The parameters of the source were chosen following an approach of an equivalent piston source: The effective diameter was chosen by fitting the geometry of the measured axial distribution in the focal region or in the last diffraction lobe; the source amplitude was chosen to match the corresponding pressure value at the focus or the last diffraction maximum.[13–15] The ENRAF transducer was modeled as a flat uniformly vibrating piston; the ICR and Sonic Concepts transducers were modeled as sections of a uniformly vibrating spherical shell. This paper is not particularly concerned with the differences between the measurements and modeling, which are typically due to a non-uniform surface vibration even of the simplest single element transducers.[16] This non-uniformity is mainly caused by Lamb wave generation at transducer surface, housing, wiring, and other construction details. The actual vibration pattern of the transducer can be reconstructed using the acoustic holography (or otherwise called back projection) method not employed in this work.[17] Here, the modeling results are given primarily for illustrative purposes and as a check of the hydrophone measurements of pressure variation around the focus or last-axial maximum.

III. EXPERIMENTAL RESULTS

A. Measurements of the ultrasound field of the flat physiotherapy transducer

Pressure distributions in the field of the flat physiotherapy transducer, modeled and measured with the hydrophone in water along the beam axis, are shown in Fig. 4. In the modeling, the amplitude-phase distribution at the radiator surface was considered to be uniform and the corresponding pressure distribution along the axis in water was calculated using the Rayleigh integral. The modeling data were normalized to match the pressure value at the last diffraction maximum in the measured field. The dashed vertical lines in Fig. 4 correspond to the planes of the IR measurement $z = 10$, 25, 30, 50, 70, 81, and 90 mm. Bold gray vertical lines correspond to the planes of hydrophone scanning $z = 25$ and 81 mm. Although the pressure distribution measured in the near-field of the transducer does not follow the structure of the field for an ideal piston source, the results of measurements are in better agreement with the modeling within the last diffraction lobe of the beam.

The calibration coefficient (3) $k/h = 0.025$ levels·m^2/W·s was determined as a ratio of the maximum values in the IR and hydrophone measurements made in the plane of the last diffraction maximum ($z = 81$ mm). Corresponding intensity distributions, measured with the hydrophone and reconstructed from the IR measurements, are shown in Figs. 5(a)

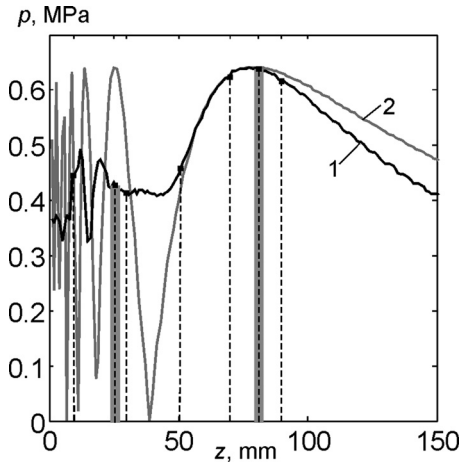

FIG. 4. Axial pressure distribution of the flat physiotherapy transducer measured with the hydrophone (1) and calculated for a piston source (2). Dashed vertical lines correspond to the planes of IR measurement $z = 10$, 25, 30, 50, 70, 81, and 90 mm. Bold gray vertical lines correspond to the planes of hydrophone scanning $z = 25$ and 81 mm.

and 5(b). One-dimensional distributions of the corresponding quantities in the same plane over the coordinate y are compared in Fig. 5(c). The spatial structure and the dimensions of the intensity distributions obtained from both IR and hydrophone measurements are in very good agreement: The beam widths at −3 dB level are 5.5 mm for the IR measurements and 5.75 mm for the hydrophone measurements.

The calibration coefficient obtained at a distance $z = 81$ mm was then used to reconstruct quantitative distribution of intensity from the IR measurements in the plane $z = 25$ mm. The results of the reconstruction are compared with the hydrophone measurements in the same plane in Figs. 5(d)–5(f). At this distance close to the transducer, the ultrasound field shows some stepped spatial structure and is about half the amplitude at the maximum (Fig. 4). The signal-to-noise level in IR measurements is therefore lower and limited precision in positioning of the absorber in the oscillating near-field of the transducer has a stronger effect. However, although some discrepancies in the IR and hydrophone-measured distributions are present at this distance, the results still agree well, especially considering the uncertainty in axial distance and the steps shown in the intensity profile, one of which occurs close to the −3 dB level: The beam widths at −3 dB level are 8.8 mm for the IR measurements and 7.2 mm for the hydrophone measurements.

Measurements with a thin 2 mm absorber enable reconstruction of intensity distributions over a large range of distances from the transducer, almost to perform a three-dimensional (3D) reconstruction of the field by moving the absorber with small spatial steps along the z axis. As an example, 2D spatial distributions of intensity measured at the planes $z = 10$ mm (a); 30 mm (b); 50 mm (c); 70 mm (d); and 90 mm (e) with the IR camera are presented in Fig. 6. The distributions are normalized to the maximum value I_{max} of each plot and the contour lines are given with the step of 0.2 I_{max}.

B. Measurements of the ultrasound field of the focused ICR radiator

Following the presentation used in Sec. III A, distributions of the pressure amplitude of the ICR transducer, modeled and measured with the hydrophone along its axis, are shown in Fig. 7. A uniformly vibrating focused source was considered as a boundary condition for the modeling. Again, dashed vertical lines correspond to the planes of the IR measurement (this time for $z = 50$, 70, 80, 90, 110, 120, and 130 mm). Bold gray vertical lines correspond to the planes of the hydrophone scanning $z = 80$ and 120 mm. Pressure distributions obtained in measurement and modeling are practically the same in the region of the main focal lobe. However, some disagreement is observed in the prefocal area of the transducer that is caused by the nonuniform

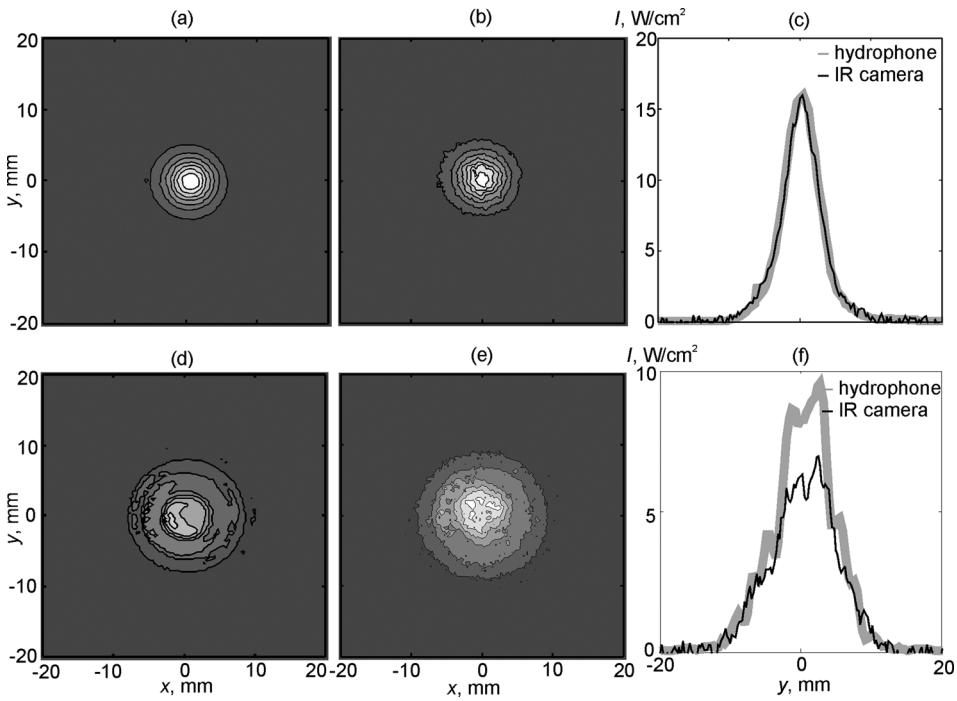

FIG. 5. Spatial distributions of intensity in the field of the flat physiotherapy transducer, measured at the plane $z = 81$ mm (top row) and $z = 25$ mm (bottom row) with the hydrophone [(a) and (d)] and IR camera [(b) and (e)]. Contour lines are given with increments of 2 W/cm² [(a) and (b)] and 1 W/cm² [(d) and (e)]. Intensity distributions measured along the y axis ($x = 0$) in the same planes with the hydrophone (▬) and IR camera (—) [(c) and (f)].

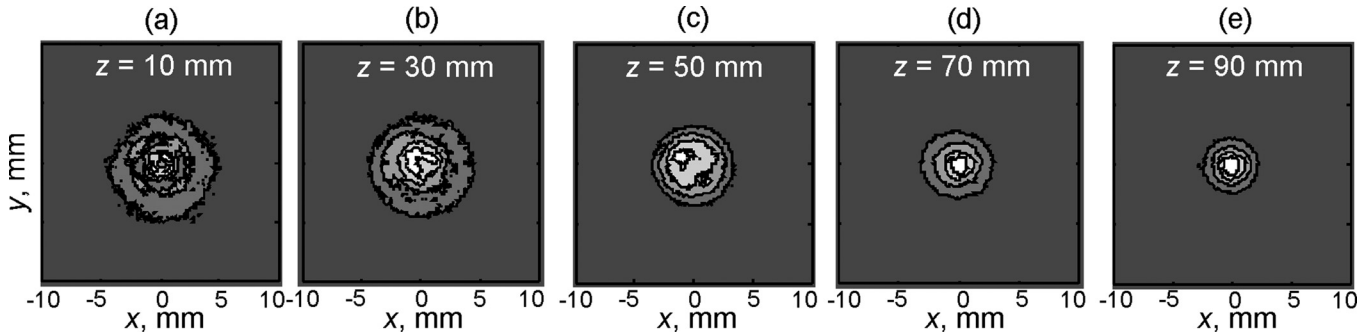

FIG. 6. Spatial distributions of intensity in the field of the flat physiotherapy transducer, measured with the IR camera at the planes: (a) $z = 10$ mm; (b) 30 mm; (c) 50 mm; (d) 70 mm; and (e) 90 mm. The distributions are normalized to the maximum value I_{max} in each plot. Contour lines are given with the step of 0.2 I_{max}.

distribution of the oscillation velocity at the surface of the real transducer in the experiment and the presence of the rim surrounding the transducer [see Fig. 3(c)].

For the focused ICR transducer, the calibration coefficient (3) was obtained from the IR measurement and hydrophone scanning in the focal plane at $z = 120$ mm, where calculation of the ratio of the maximum values in the distributions gave $k/h = 0.035$ levels·m^2/W·s. Spatial distributions of intensity, obtained from the hydrophone scanning (a) and IR estimates (b) in the same plane at 120 mm are shown in Figs. 8(a) and 8(b). The distributions are in very good agreement, which can be seen in more detail in Fig. 8(c), where one-dimensional intensity distributions are plotted over the coordinate y: The beam widths are 2.375 mm for the IR measurements and 2.4 mm for the hydrophone measurements.

Using the same calibration coefficient, the intensity distribution was reconstructed from the IR image and compared with the results of the hydrophone scanning in another plane $z = 80$ mm [Figs. 8(d)–8(f)]. Figure 8 shows that the absolute values of intensity, spatial structure, the number of peaks and their amplitudes, are again in good agreement, especially considering the steps shown in the profile and the uncertainty in axial distance: The beam widths at −3 dB level are

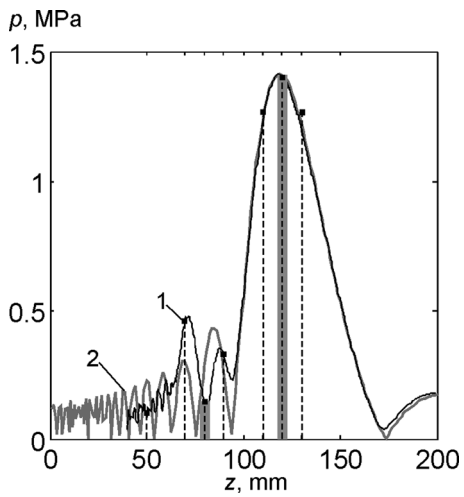

FIG. 7. Axial pressure distribution of the focused ICR transducer measured with the hydrophone (1) and calculated for the focused piston source model (2). Dashed vertical lines correspond to the planes of the IR measurement $z = 50, 70, 80, 90, 110, 120, 130$ mm. Bold gray vertical lines correspond to the planes of the hydrophone scanning $z = 80$ and 120 mm.

16.1 mm for the IR measurements and 14.5 mm for the hydrophone measurements.

The ability to realize 3D scanning of the ultrasound field using IR camera measurements for the ICR transducer is illustrated in Fig. 9. The transducer was moved from the distance $z = 40$ mm to $z = 140$ mm with the spatial increment $\Delta z = 2$ mm and selected frames of intensity distribution, measured at the planes $z = 50$ mm (a); 70 mm (b); 90 mm (c); 110 mm (d); and 130 mm (e) are presented in the figure. The distributions are normalized to the corresponding maximum values of I_{max} in each plot and the contour lines are given with the step of 0.2 I_{max}.

C. Measurements of the ultrasound field of the focused radiator Sonic Concepts H101

The last set of measurements was carried out for the focused transducer Sonic Concepts H101. Similarly to the results obtained in Secs. III A and III B, pressure distributions of the Sonic Concepts transducer were modeled and measured with the hydrophone along its axis (Fig. 10). Again, dashed vertical lines correspond to the planes of the IR measurement (this time, $z = 42$, 50, 54, 62, and 82 mm). Bold gray vertical lines correspond to the planes of the hydrophone scanning $z = 50$, 54, and 62 mm. A qualitatively good agreement is observed in the main focal lobe and over three prefocal lobes. Some discrepancies in the near field are due to the limitation of the assumption on the uniform distribution of the oscillation velocity at the transducer surface in the modeling.

The calibration coefficient (3) $k/h = 0.035$ levels·m^2/W·s, was obtained from the IR measurement and hydrophone scanning in the focal plane at $z = 62$ mm. In Fig. 11(a) the corresponding one-dimensional intensity distributions, calculated from the hydrophone measurements and from the IR image are presented. The same beam widths (1.375 mm for the IR measurements and 1.4 mm for the hydrophone measurements) and similar spatial structure are observed.

The same calibration coefficient was then applied to reconstruct the intensity distribution from the IR measurements in the planes of the first diffraction minimum ($z = 54$ mm) and maximum ($z = 50$ mm). The corresponding intensity distributions compared to their hydrophone scans are presented in Figs. 11(b) and 11(c). In both cases some deviations are observed in the absolute intensity values, although the spatial structure and the width of the lobes look

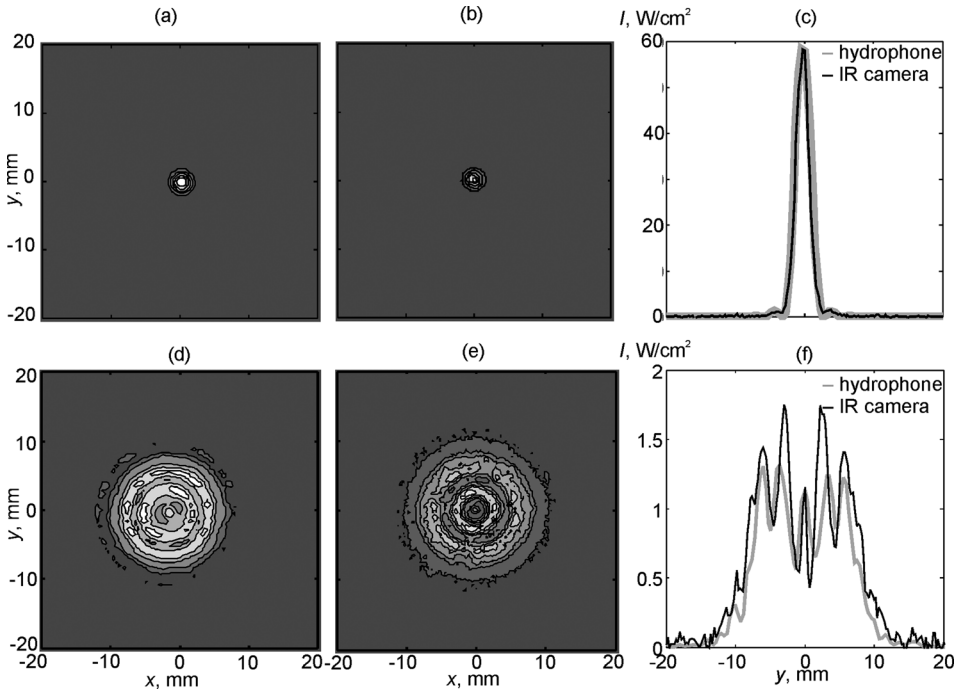

FIG. 8. Spatial distributions of intensity in the field of the ICR transducer, measured at the focal plane $z = 120$ mm (top row) and at the distance $z = 80$ mm (bottom row) with the hydrophone [(a) and (d)] and IR camera [(b) and (e)]. Contour lines are given with the step 10 W/cm^2 [(a) and (b)] and 0.25 W/cm^2 [(d) and (e)]. Intensity distributions measured along the y axis ($x = 0$) in the same planes with the hydrophone (▬) and IR camera (—) [(c) and (f)].

quite similar. The scan at 54 mm shows substantial differences at the local maxima and minimum but is much closer at intermediate locations. These could perhaps be thermal conduction effects but the scan at 50 mm shows very good agreement everywhere. At 50 mm the beam widths at −3 dB level are the same, 1.27 mm, for the IR measurements and the hydrophone measurements. At 54 mm the beam widths at −3 dB level are very close: 2.03 mm (left lobe) and 2.25 mm (right lobe) for the IR measurements and 2.04 mm (left lobe) and 2.27 mm (right lobe) for the hydrophone measurements. It is noticeable that the agreement away from the focus is better with this transducer than the other two. This may be because we chose specific features of the field (local minimum and local maximum at 55 and 50 mm, respectively) to define the measurement planes and were able to locate these features using both the hydrophone and the IR camera, leading to much smaller uncertainties in establishing the correct distance for comparison.

As in Secs. III A and III B, 3D reconstruction of the intensity field was performed using the IR camera and moving the transducer over a large range of distances from the absorber. The examples of the intensity distributions measured at the different planes are presented in Fig. 12. The distributions are normalized to their maximum values I_{max} and the contour lines are given with the step of 0.2 I_{max}.

IV. DISCUSSION

The main goal of this paper was to test the suitability of the IR method for rapid assessment of absolute values of the intensity in acoustic fields radiated by different medical ultrasound transducers. Three transducers were investigated: A flat physiotherapy transducer and two focused HIFU transducers. Calibration coefficients between IR measurement data *versus* hydrophone data were determined at one selected plane for each transducer and allowed further conversion of IR measurements to intensity distributions in other planes of measurement. Experimentally obtained data from IR measurements and hydrophone scans displayed a good correlation. In the following discussion, several factors of relevance to IR mapping are raised, many in a rather general way so that the reader interested in implementing such a method will be aware of them and can consider how these factors are likely to influence their own intended studies.

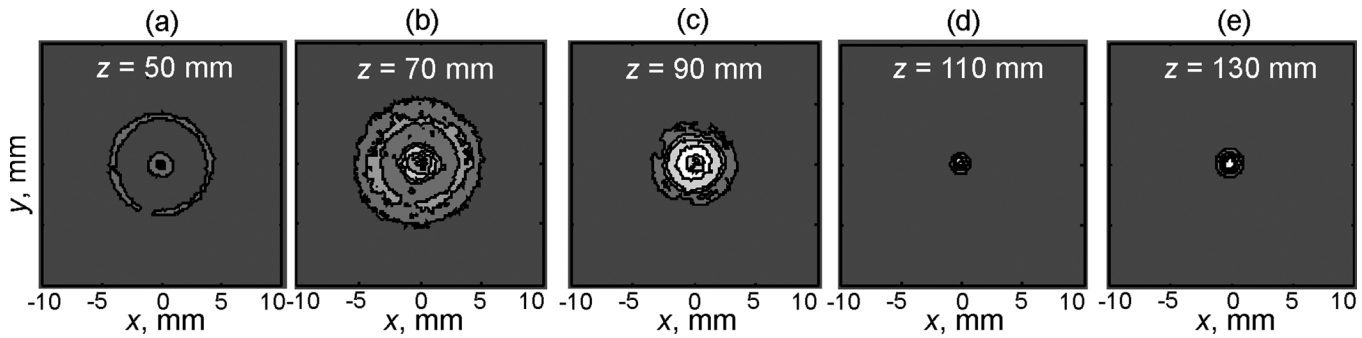

FIG. 9. Spatial distributions of the intensity in the field of the ICR transducer, measured at the planes: (a) $z = 50$ mm; (b) 70 mm; (c) 90 mm; (d) 110 mm; (e) 130 mm with the IR camera. The distributions are normalized to their maximum value I_{max}. Contour lines are given with the step of 0.2 I_{max}.

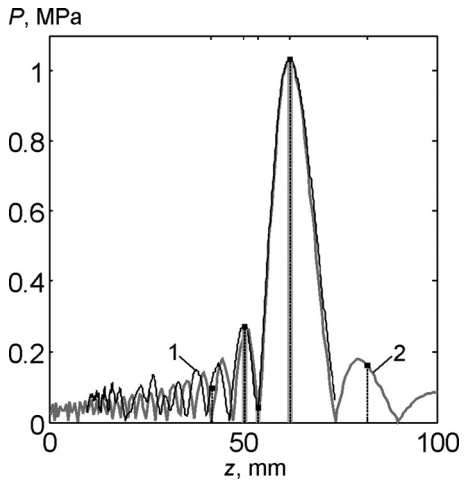

FIG. 10. Axial pressure distributions for the focused transducer Sonic Concepts H101, measured with the hydrophone (1) and calculated for the uniform piston source model (2). Dashed vertical lines correspond to the planes of IR measurement $z = 42$, 50, 54, 62, and 82 mm. Bold gray vertical lines correspond to the planes of hydrophone scanning $z = 50$, 54, and 62 mm.

An essential feature of the IR method tested here was to employ a thin (2 mm) highly absorbing (6 dB losses one way) layer for 2D acoustic field reconstruction. Compared to other experimental configurations, for example, using a thick (4 cm) gel phantom,[9] thin absorber enables field mapping down to distances almost touching the transducer. It is also possible to carry out faster mapping by moving quickly from one plane to the next as the cooling time of the thin absorber between insonations was less than 5 s, thus enabling 3D field reconstruction on the time scale of minutes. The choice of material parameters of the absorber and its thickness was a compromise between competing effects and there is no doubt scope to further optimize the absorber. For example: A high overall absorption in a layer leads to a high conversion efficiency close to the air interface but also means that the overall transmission through the layer is small. A good impedance match to water reduces the reflection from the water/absorber interface but a high absorption coefficient is equivalent to a large imaginary component of sound speed, which leads to poorer matching with water. A high absorption coefficient also leads to a high thermal gradient through the thickness of the absorber, which complicates the heat flow. A low thermal conductivity and low volumetric heat capacity are preferable to reduce thermal diffusion and increase sensitivity, respectively. However, while high sensitivity is good for measuring relatively low intensity fields, it means that very high temperature rises will be generated in high intensity fields. Since many material properties are temperature sensitive, this in turn means that the behavior of the absorber (especially the absorption coefficient and transmission loss) could change significantly during an insonation. So, at least in principle, the ideal measurement setup for physiotherapy transducers may be different from the ideal setup for clinical HIFU transducers.

The absorber must also be available in a suitable format. At NPL, a number of acoustic materials have been developed for different ultrasonic and underwater acoustic applications. Of these F28 was the most convenient since it is available in two-part liquid sachets (type F36, Precision Acoustics Ltd, Dorchester, UK) which can be mixed and cast into layers of any preferred size and thickness. The acoustic properties offered a good compromise of high absorption and good matching to water. For these studies, the material was cast in a sheet 2 mm thick providing a one-way transmission loss of approximately 6 dB at 1 MHz. Almost all materials show an absorption coefficient which increases proportionally to frequency or more rapidly. So a particular thickness of absorber is only suitable for a narrow range of frequencies: Thinner layers should be used for higher frequencies. An attempt to use the same absorber when driving the ICR transducer at its third harmonic resulted in images after 0.2 s which were hardly distinguishable from noise. Furthermore, heating caused by harmonics in a nonlinear beam will be reduced in the IR image relative to the fundamental. A low level driving voltage of the transducers therefore was used in this study to avoid significant nonlinear harmonic generation effects: This approach is also commonly used for hydrophone measurements of HIFU fields to avoid damage and is part of the measurement process for the draft IEC Technical Specification IEC65556.[18]

The absorber properties vary with temperature and, in particular, the absorption coefficient (and hence the transmission coefficient) is quite a strong function of temperature. The absorption coefficient of F28 increases from 23 dB/cm/MHz at 20 °C to 40 dB/cm/MHz at 40 °C.[19] Since the temperature inside the absorber varies with distance from the air interface (which is the measured surface) and with time, it is not straightforward to correct for changes in absorption coefficient (or any other property of the absorber). A more general procedure would be to account for this effect by

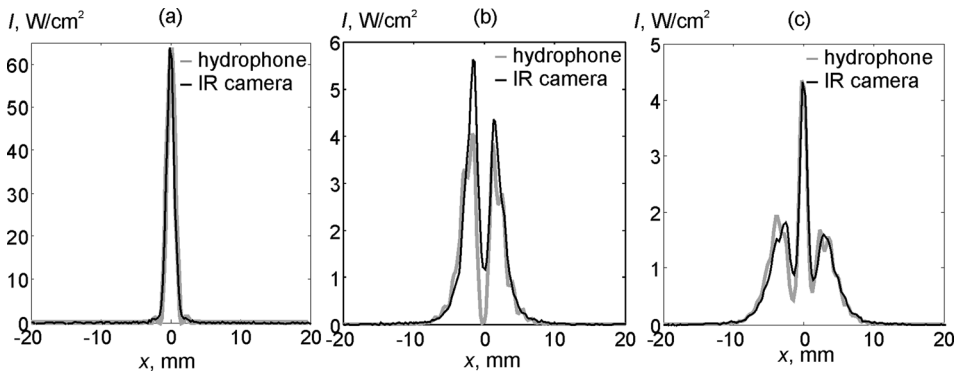

FIG. 11. Intensity distributions of the Sonic Concepts H101 transducer, measured at the focal plane $z = 62$ mm (a), at the plane of the first prefocal minimum $z = 54$ mm (b), and at the plane of the first prefocal maximum $z = 50$ mm (c), obtained from the hydrophone (▬) and IR camera (—) measurements.

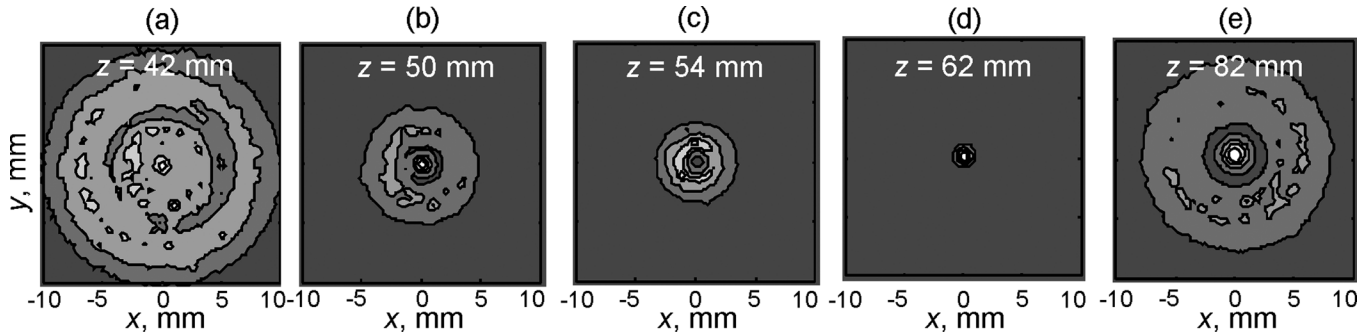

FIG. 12. 2D intensity distribution of the Sonic Concepts H101 transducer, measured with the IR camera at the planes: (a) $z = 42$ mm; (b) 50 mm: focal plane; (c) 54 mm: Plane of the first prefocal minimum; (d) 62 mm: Plane of the first prefocal maximum; and (e) 82 mm. The distributions are normalized to their maximum values I_{max} in each plot. Contour lines are given with the step of 0.2 I_{max}.

determining the rate of change of temperature at the start of insonation by curve fitting rather than simply measuring the change in temperature over a fixed time interval.

Another important feature of the method employed here was the relatively short duration of the exposure in IR measurements (0.2 s). It has been shown previously that heat conduction in transverse coordinates and convection effects can be neglected in resolving spatial inhomogeneities of sub-millimeter size in intensity distributions by using only sub-second exposure periods.[6,8] A simple estimation of the diffusion time t_{diff} in a lateral direction for a temperature inhomogeneity of radius a is $t_{diff} = a^2/4\chi$, where χ is the thermal diffusivity of the material.[20,21] For the material F28, $\chi = 1.9 \cdot 10^{-7}$ m^2 s^{-1} and a diffusion time of 0.2 s corresponds to a field inhomogeneity of $2a = 0.8$ mm in size. The temperature increase thus will be almost linear with time for intensity inhomogeneities of about 1 mm size with 0.2 s exposures. Meanwhile, if the experimental conditions permit, it is worthwhile to further reduce the exposure to minimize the influence of heat conduction effects and to resolve fine spatial structure of intensity distributions.

Multiple reflections between the transducer and absorber because of the presence of water/absorber and absorber/air interfaces may cause artifacts in the measurements. These reflections are relatively weak as the double-pass transmission loss in the absorber is 12 dB and reflection from water/absorber interface is −25 dB. However, depending on the relative phase, the interference of the direct and reflected waves may cause a modulation in the intensity distribution which is sensitive to small changes of less than a quarter wavelength in distance between the transducer and the absorber. The use of a tone burst regime with the correct timing allowed suppression of this coherent self-interference which is especially important for measurements in the near fields of transducers with fine spatial structure. Figure 13 illustrates the advantages of tone burst excitation for the ICR transducer. Three images on the left show the temperature distribution measured with CW excitation at a distance of approximately 70 mm; the distance for each image differs from the previous one by only 40 μm. Shown on the right are the equivalent images measured under tone burst excitation such that the reflected wave does not overlap in time with the direct wave. Some features in the distributions on the left are very sensitive to distance, whereas those on the right are clearly much more consistent. The significance of interference will depend on the relative magnitude of the direct and reflected waves and, consequently, on the transducer geometry and the distance from the absorber. In a focused field for measurements close to the focus, the amplitude of the direct wave will be much larger than the reflected wave so the effects of interference will be less significant.

In this work, the burst repetition period was chosen as $6z/c$, and the burst duration was $2.4 \cdot z/c$ (0.4 duty factor)

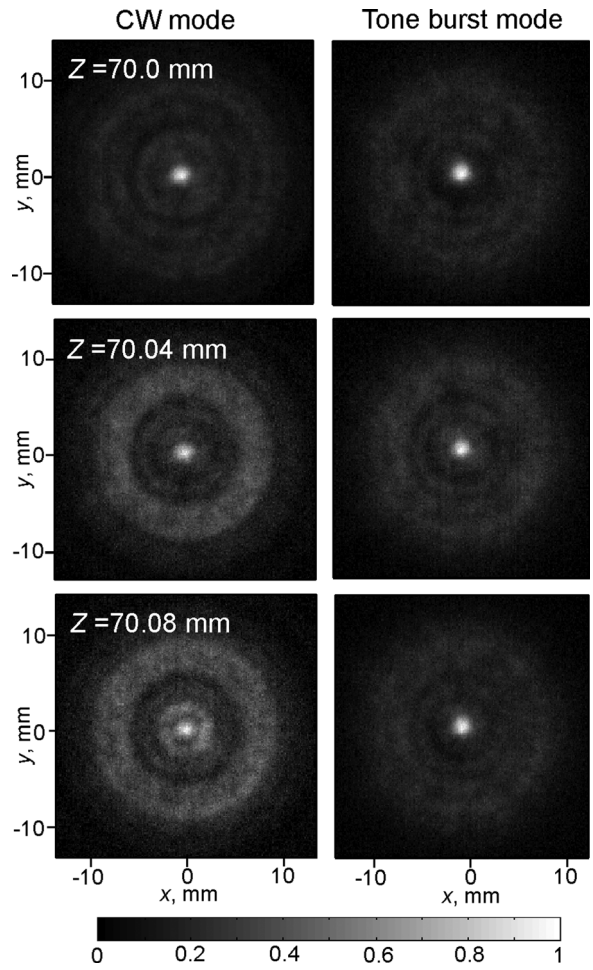

FIG. 13. Temperature distributions measured for the ICR transducer in x-y planes at intervals of 40 μm along the z axis of the beam: CW insonation (on the left) and tone burst insonation (on the right).

where z is the distance between the reflecting interface and the transducer. This choice was actually based on a miscalculation leading to a small temporal overlap between the incident and reflected waves. To completely avoid self-interference inside the absorber, the burst duration must be less than $2z/c$; and to avoid overlap with the next tone burst at the transducer, the repetition period must be greater than $4z/c$. The maximum duty factor permitted is therefore 0.5 which will reduce the signal-to-noise ratio. However, if the temperature rise is high, smaller duty factors can be used by increasing the repetition period or decreasing the burst duration. Note that in order to compare directly the measurements at different distances z, the results must be scaled to the same duty factor.

Some transducers take a number of cycles to reach full output: This effect is sometimes known as "ring-up." The effect is to reduce time-average acoustic intensity when short burst durations are used and therefore to limit the minimum measurement distance. For instance, if a 1 MHz transducer takes 20 cycles to reach full output, a tone burst must obviously be at least 20 cycles (20 μs) long and the distance z must be at least 15 mm. In fact, because of the ring-up time, the energy in a 20 cycle burst is much less than, for instance, 10% of that in a 200 cycle burst: This systematic effect is well known when measuring total power under short tone burst conditions.[22] Using tone burst excitation for IR field measurement (as opposed to relative mapping in a single plane) therefore introduces a systematic bias which, for some transducers, may be significant even for quite long tone bursts. For instance, if the pressure amplitude in a tone burst of frequency f grows with time following the envelope of the error function erf($t \cdot f/5$), the pressure amplitude is close to its maximum value after ten cycles [Fig. 14(a)]. However, due to the energy that is lost at the beginning of the tone burst [Fig. 14(b)], the time-average intensity only reaches 60% of its CW value after 10 cycles [Fig. 14(c)]. Even after

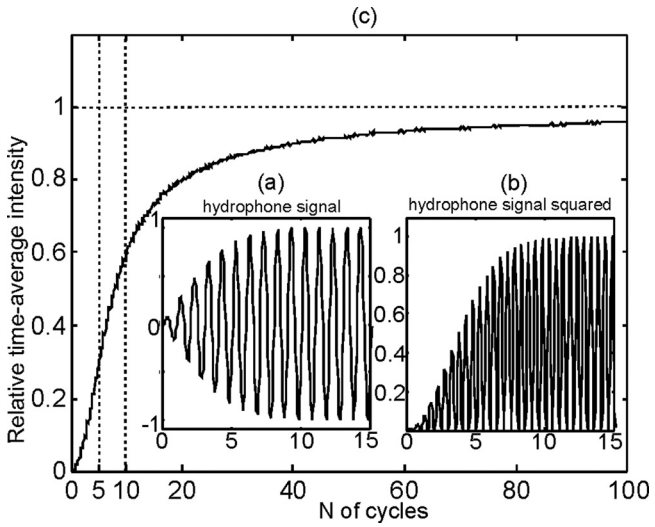

FIG. 14. Illustration of the systematic reduction in time-average intensity when using tone burst mode of insonation and reducing the burst duration. (a) Pressure amplitude distribution from the hydrophone signal; (b) pressure amplitude squared distribution i.e., relative energy distribution; (c) relative time-average intensity distribution.

100 cycles (20 times the ring-up time) it has only reached 96% of the continuous value. Of course, the specific values depend on the form assumed for the ring-up envelope function but clearly caution is required when using tone burst measurements to determine CW field quantities and vice versa. To account for this effect, a correction factor can be introduced to the IR measurements of intensity if short tone bursts are used similar to the measurements of total power output (for instance with a radiation force balance) under short tone burst conditions.[23]

Change in IR emission from a body is not linearly related to its temperature. When an IR camera generates temperature maps, the nonlinear relationship should already be accounted for within the camera firmware and software. However, when calculating a change in temperature by subtracting raw IR images, as we have done with the system described in this paper, the relationship between the temperature and the signal received by the camera should be explicitly included in the algorithm. Since IR flux is proportional to the surface emissivity and to the fourth power of absolute temperature,[24] it can be shown that the increase in the IR emission A_{IR} for a temperature increase δT is $A_{\mathrm{IR}} \approx 4T_0^3 C\varepsilon\delta T(1 + 1.5\delta T/T_0 + ...)$, where T_0 is the initial object temperature (K), ε is the surface emissivity, and C is a device specific constant. Consequently, at room temperature, there is a deviation from strict proportionality of about 1.5% for a temperature rise of 3 °C. This increases to 15% for a 30 °C rise and 30% for a 60 °C rise. A_{IR} is also strongly dependent on the initial temperature: One should be aware of this source of nonlinearity when carrying out simple raw image subtraction and correct for it on a pixel-by-pixel basis if the temperature of the absorber varies by more than about 3 °C.

The significance on the heat source function of interference between the incident and reflected wave close to the air interface has been studied by Myers and Giridhar *et al.*[9,10] In their analysis, since the reflected wave is inverted, the pressure at the interface itself is always zero and the pressure amplitude at $\lambda/4$ from the interface is nearly double the incident pressure. Following Nyborg,[25] the time-averaged local heat source function, $\langle Q_v(r)\rangle$, was calculated as being determined by the local pressure amplitude, $p(r)$, absorption coefficient α, density ρ, and sound speed c of the medium: $\langle Q_v(r)\rangle = 2\alpha p(r)^2/\rho c$. The heating of the interface is therefore not caused by the absorption of ultrasound, which is equal to zero at the interface, but by thermal conduction from a region of very strong heat sources at the pressure antinode $\lambda/4$ distant.

In one-directional plane wave propagation in a homogeneous thermoviscous medium (no interface) the rate of temperature rise with time t is $T = 2\alpha t p(z)^2/(C_v\rho c)$, where z is the propagation coordinate and C_v is the volumetric heat capacity of the medium. The spatial modulation caused by interference results in a different time dependency[9,10] which can be written as

$$T = 2\left\{1 - \frac{1 - \exp(-4k^2\chi t)}{4k^2\chi t}\right\} 2\alpha t p(r)^2/(C_v\rho c). \qquad (4)$$

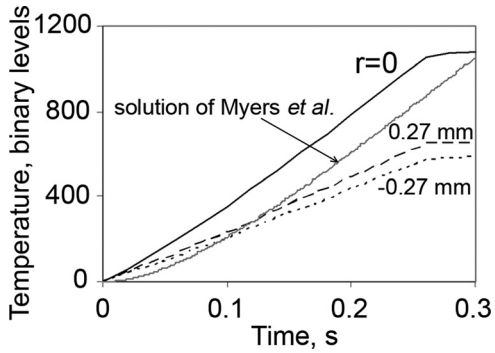

FIG. 15. IR signal in binary levels *versus* time measured at the focal plane of the ICR transducer [Fig. 8(c)] on the axis ($r=0$, solid curve) and at 0.27 mm (dashed) and −0.27 mm (short dashed) off axis. Analytic solution of Myers *et al.* (Ref. 9) with parameters $\chi=1.92\cdot10^{-7}$ m^2/s (temperature conductivity) and $k=4186\,\mathrm{m}^{-1}$ (wave number) that correspond to our experiment is plotted in gray color. The solution is scaled so that the temperature slope after 0.2 s is approximately the same as in the experiment at $r=0$.

The extra factor in curly brackets arises from the spatial modulation and the factor of 2 arises from the double pass of the acoustic wave through the medium. In this case, in our experimental conditions of 1 MHz frequency (wave number $k=4186\,\mathrm{m}^{-1}$) and temperature conductivity of the F28 absorber ($\chi=1.92\cdot10^{-7}$ m^2/s), the rate of change of temperature almost matches the unmodulated case after 0.15 s. The change in temperature between 0.02 and 0.22 s (corresponding to our measurements) is 77% of the unmodulated value: This effect therefore becomes just one contribution to the overall, empirically determined calibration factor. However, it is worth pointing out that we have not observed this type of steepening curve close to the center of a beam, which suggests that the analysis of Myers and Giradhar is not appropriate to our setup. Figure 15 shows the solution, Eq. (4), as a function of time up to 0.3 s for the F28 absorber compared to the measured IR signal of the ICR silver transducer in the focal plane [Fig. 8(c)]. The Myers and Giridhar calculation, Eq. (4) is normalized by setting the slope at 0.2 s to be the same as the measured slope on the beam axis, $r=0$. Contrary to the steepening of the predicted curve, the measured slope is almost constant: There is a small increasing trend and it can be seen that after 0.25 s when insonation stops, the temperature continues to increase. This would be expected even without interference because the temperature inside the absorber in front of the interface will be higher than the temperature at the interface even in a progressive wave due to the high attenuation of the absorber. We speculate that the reason for this difference in our measurements as compared to theoretical predictions is perhaps the model is flawed for this setup or perhaps the camera may measure the temperature integrated over a depth of 100 to 400 μm, i.e., it may perform spatial averaging along the z-coordinate.

An automated system is under development at NPL which will include the aspects described in this discussion and further work is planned to study the frequency dependence of the properties of absorber parameters, the optical properties of the absorber in the infra-red region, to evaluate the effect of temperature dependence of acoustic and thermal properties of the absorber, to optimize the material properties of the layer (absorption coefficient, impedance) and its thickness, to investigate the stability of acoustic and thermal properties of the absorber with time and temperature, and to evaluate the maximum temperature rise that can be reached for a particular absorber without damaging it.

V. CONCLUSION

An acoustic absorbing layer of 2 mm thickness was tested and calibrated to provide measurements of the intensity of 1 MHz ultrasound fields using an IR camera. Calibration was carried out by comparing IR data with hydrophone measurements. It was shown that the method provides fast maps of intensity distributions whose shapes agreed well qualitatively with hydrophone measurements: Measured beam widths were typically within 1.5 mm at the near-field locations and much closer in the plane of the maximum. In terms of absolute sensitivity, results were reasonably consistent for three transducers of different geometries measured close to the focus or last axial maximum: The average calibration factor was 0.031 levels·m^2/W·s with a range of ±20%. There are larger differences in sensitivity (up to a factor of 2 from the mean value) at other locations, the reasons for which are not clear yet but will be further explored. Since the acoustic field changes rapidly in the near field, a significant part of the observed difference may simply be due to the practical difficulty of ensuring that hydrophone and IR measurements in the near field are made at the same distance. The transmission loss of the absorber layer was 6 dB and this seems to be a good compromise allowing sufficient heating for IR measurements even for intensities below 0.1 W/cm^2. For higher frequency fields, a thinner layer would be required to have the same 6 dB attenuation. Tone burst excitation is preferred to minimize the interference of the reflections from the transducer but may not always be necessary for focused transducers measured close to the focus.

Based on the methods and discussion presented in this paper, the following two outline procedures (one simpler, one more accurate) are recommended to estimate time-average intensity distributions.

Initially, for both procedures:

(1) The absorber is calibrated at the frequency of interest.
(2) The transducer is driven in tone burst mode with burst duration and repetition period chosen according to the range of distances required.
(3) An overall insonation time of 0.2 s is generally suitable but at high intensity levels it should be adjusted to avoid overheating the absorber, as well as burst duration and repetition period.
(4) A reference image is taken immediately before or immediately after the start of insonation (preferably within 20 ms).

Then, to follow the simpler procedure:

(5.1) One field image is taken at known time after the reference image.

(6.1) The reference image is subtracted from the field image and divided by the time between images to calculate the map of the initial rate of change of signal.
(7.1) The corrected rate of change map is divided by the calibration factor to determine the intensity map.

Or, to follow the more accurate route:

(5.2) A sequence of field images is taken at known times after the reference image.
(6.2) The reference image is subtracted from each of the field images.
(7.2) The sequence of subtracted images is analyzed using a pixel-by-pixel curve fitting routine to calculate the map of the initial rate of change of signal.
(8.2) Corrections for ring-up and initial absorber temperature are calculated and then applied if necessary.
(9.2) The corrected rate of change map is divided by the calibration factor to determine the intensity map.

The IR system described in this paper was able to map in good detail focused and unfocused ultrasound fields with millimeter-sized structure and with local time average intensity from below $0.1\,W/cm^2$ to at least $50\,W/cm^2$. Significantly higher intensities could be measured simply by reducing the duty cycle.

ACKNOWLEDGMENTS

This work was supported in part by the European Metrology Research Programme (Joint Research Project HLT03, which is jointly funded by the EMRP participating countries within EURAMET and the European Union), by the National Institutes of Health (Project No. EB007643), by the Russian Foundation for Basic Research (Project Nos. 12-02-00028 and 12-02-31388), and by the Acoustics and Ionizing Radiation program of the UK National Measurement Office. The authors gratefully acknowledge the help of John Nunn for the loan of the IR camera, Gail ter Haar for the loan of one of the transducers and Oleg Sapozhnikov for helpful discussions.

[1]IEC/TR 62649 Edition 1.0, "Requirements for measurement standards for high intensity therapeutic ultrasound (HITU) devices," Technical Report, International Electrotechnical Commission, Geneva (2010).
[2]A. Shaw and M. Hodnett, "Measurement and calibration issues for therapeutic ultrasound," Ultrasonics **48**, 234–252 (2008).
[3]G. ter Haar and P. Carnochan, "A comparison of ultrasonic irradiation and RF inductive heating for clinical localized hyperthermia applications," Br. J. Cancer **45**(Suppl. V), 77–81 (1982).
[4]T. Pashovkin, E. Khizhnyak, and A. Sarvazyan, "Thermographic investigation of ultrasonically induced temperature distribution in tissues and tissue-equivalent phantoms," Archives Acoust. **9**(1–2), 15–22 (1984).
[5]V. A. Khokhlova, N. Miller, R. Ollos, R. W. Martin, M. R. Bailey, Y. Mohammadian, and M. Naghavi, "Visualization of temperature rise induced by high intensity ultrasound in tissue," in *Proceedings of the 17th International Congress on Acoustics*, Rome University "La Sapienza," Vol. 7, pp. 186–187 (2002).
[6]J. W. Hand, A. Shaw, N. Sadhoo, S. Rajagopal, R. J. Dickinson, and L. R. Gavrilov, "A random phased array device for delivery of high intensity focused ultrasound," Phys. Med. Biol. **54**, 5675–5693 (2009).
[7]A. Shaw and J. Nunn, "The feasibility of an infrared system for real-time visualization and mapping of ultrasound fields," Phys. Med. Biol. **55**, 321–327 (2010).
[8]S. Bobkova, L. Gavrilov, V. Khokhlova, A. Shaw, and J. Hand, "Focusing of high-intensity ultrasound through the rib cage using a therapeutic random phased array," Ultrasound Med. Biol. **36**, 888–906 (2010).
[9]M. R. Myers and D. Giridhar, "Theoretical framework for quantitatively estimating ultrasound beam intensities using infrared thermography," J. Acoust. Soc. Am. **129**, 4073–4083 (2011).
[10]D. Giridhar, R. A. Robinson, Yu. Liu, J. Sliwa, V. Zderic, and M. R. Myers, "Quantitative estimation of ultrasound beam intensities using infrared thermography—Experimental validation," J. Acoust. Soc. Am. **131**, 4283–4291 (2012).
[11]S. Bobkova, A. Shaw, L. Gavrilov, V. Khokhlova, and J. Hand, "Feasibility of HIFU tissue ablation in the presence of ribs using a 2D random phased array," in *Proceedings of the 9th International Symposium On Therapeutic Ultrasound* (AIP Physics Conference Proceedings), pp. 27–30 (2010).
[12]A. Shaw, V. Khokhlova, S. Bobkova, L. Gavrilov, and J. Hand, "Calibration of HIFU intensity fields measured using an infra-red camera," *Proceedings of AMUM 2010*, J. Phys.: Conf. Ser. No. 279, Ref. 012019 (2011).
[13]V. A. Khokhlova, R. Souchon, J. Tavakkoli, O. A. Sapozhnikov, and D. Cathignol, "Numerical modeling of finite amplitude sound beams: Shock formation in the near field of a cw plane piston source," J. Acoust. Soc. Am. **110**(1), 95–108 (2001).
[14]M. S. Canney, M. R. Bailey, L. A. Crum, V. A. Khokhlova, and O. A. Sapozhnikov, "Acoustic characterization of high intensity focused ultrasound fields: A combined measurement and modeling approach," J. Acoust. Soc. Am. **124**(4), 2406–2420 (2008).
[15]O. V. Bessonova and V. Wilkens, "Membrane hydrophone measurement and numerical simulation of HIFU fields up to developed shock regimes," IEEE Trans. Ultrason. Ferroelectr. Freq. Control **60**(2), 290–300 (2013).
[16]D. Cathignol, O. A. Sapozhnikov, and J. Zhang, "Lamb waves in piezoelectric focused radiator as a reason for discrepancy between O'Neil formula and experiment," J. Acoust. Soc. Am. **101**(3), 1286–1297 (1997).
[17]O. A. Sapozhnikov, Y. A. Pishchalnikov, and A. V. Morozov, "Reconstruction of the normal velocity distribution on the surface of an ultrasonic transducer from the acoustic pressure measured on a reference surface," Acoust. Phys. **49**(3), 354–360 (2003).
[18]IEC/TS 62556, "Surgical systems—Specification and measurement of field parameters for High Intensity Therapeutic Ultrasound (HITU) transducers and systems," Draft Technical Specification, International Electrotechnical Commission, Geneva (2012)
[19]A. Shaw, "A buoyancy method for the measurement of total ultrasound power generated by HIFU transducers," Ultrasound Med. Biol. **34**, 1327–1342 (2008).
[20]P. Morse and H. Feshbach, *Methods of Theoretical Physics, Part I* (McGraw Hill, New York, 1953), p. 861.
[21]M. Canney, V. Khokhlova, O. Bessonova, M. Bailey, and L. Crum, "Shock-induced heating and millisecond boiling in gels and tissue due to high intensity focused ultrasound," Ultrasound Med. Biol. **36**, 250–267 (2010).
[22]K. V. Jenderka and V. Wilkens, "Measurement of time averaged power in HITU fields—Effects of duty cycle and target distance," Metrologia **49**, 275–278 (2012).
[23]S. Maruvada, G. R. Harris, B. A. Herman and R. L. King, "Acoustic power calibration of high-intensity focused ultrasound transducers using a radiation force technique," J. Acoust. Soc. Am. **121**(3), 1434–1439 (2007).
[24]L. Michalski, K. Eckersdorf, and J. McGhee, "Optical pyrometers," in *Temperature Measurement* (John Wiley and Sons, Chichester, UK, 1991), Chap. 7.
[25]W. L. Nyborg, "Heat generation by ultrasound in a relaxing medium," J. Acoust. Soc. Am. **70**(2), 310–312 (1981).